Effect of Cellulose Nanocrystals on Fire, Thermal and Mechanical Behavior of N,N′-Diallyl-phenylphosphoricdiamide Modified Poly(lactic acid)

Weijun Yang[1†], Xiaomin Zhao[2†], Elena Fortunati[1], Franco Dominici[1], Jose M. Kenny[1], Debora Puglia[1*] and De-Yi Wang[2*]

[1]University of Perugia, Civil and Environmental Engineering Department, Materials Engineering Center, UdR INSTM, Strada di Pentima 4, 05100 Terni, Italy
[2]IMDEA Materials Institute, C/Eric Kandel, 2, 28906 Getafe, Madrid, Spain

ABSTRACT: Presented herein is a deep investigation of the fire, mechanical and thermal performances of poly(lactic acid) (PLA)-based nanocomposites, which were obtained by combining cellulose nanocrystals (CNC) with various contents of N,N′-diallyl-phenylphosphoricdiamide (P-AA) via a two-steps masterbatch melt extrusion process (glycidyl methacrylate grafting on PLA and CNC premixing with PLA). Results have shown that the value of the limiting oxygen index (LOI) increased to 28.8% and a V-0 rating in UL94 test was obtained when 2 wt% of P-AA was added in the presence of cellulose nanocrystals (3 wt%). The incorporation of CNC induced a decrease of both PHRR and THR values in micro combustion tests; meanwhile, the nucleating and plasticization effects of CNC and P-AA were evidenced. Results from tensile tests and dynamic mechanical thermal analysis (DMA) showed that the addition of CNC importantly enhanced the mechanical performance of P-AA containing systems, while the thermal stability of the nanocomposites was slightly improved in the presence of the cellulosic nanoreinforcement.

KEYWORDS: Poly(lactic acid), cellulose nanocrystals, nanocomposites, fire retardancy, mechanical response

1 INTRODUCTION

The need for using environmentally biodegradable and eco-friendly materials in the replacement of other traditional nondegradable plastics derived from fossil fuel feedstocks is constantly directing research activities towards the investigation and use of different biopolymers in many potential applications. Poly(lactic acid) (PLA) is one of the most promising bioplastics due to its many merits that have broadened its applications, such as its biodegradability, high mechanical strength, easy processing, high degree of transparency, good appearance, and low toxicity [1, 2]. The major PLA application today is in packaging (nearly 70%); even so, the increase of other applications, especially in fibers, fabrics and long-life consumer goods, is envisaged. It can also be applied in fields such as automotive, electrical, construction materials, and aerospace, because of its natural low-cost advantage. However, since these fields have a remarkable flame retardant grade requirement, the flammability of PLA is the main drawback which limits its applications; thus, improvement in its flame retardancy is required [3]. Bourbigot and Fontaine [4] reported various approaches to enhance the flame retardancy property of PLA: (a) Blending approach, i.e., the blending of low thermally stable polymer with high thermally stable polymer increases the degradation temperature of the low thermally stable polymer; (b) Use of conventional flame retardant, i.e., mainly constituted by aluminium trihydrate (ATH), magnesium hydroxide (MDH), phosphorus-containing compounds, halogenated compounds, antimony trioxide and nitrogenated compounds which serve in gas and/or condensed phase; (c) Use of nanoparticles at low loading (3–5 wt%), since they often exhibit remarkably enhanced properties when compared with those of pure polymer. In the case of PLA-based nanocomposites, it has been reported that this

Corresponding authors: deyi.wang@imdea.org; debora.puglia@unipg.it
†Equal contribution to this work

family of composites register enhanced properties (like reduced gas permeability, reinforced flexural properties, high storage modulus both in the solid and melt states, improved heat distortion temperature, accelerated biodegradability rate) in the presence of different nanofillers. In recent years, many attempts have been carried out to improve the flame retardancy of PLA. Kiliaris and Papaspyrides [5] reviewed the utilization of layered silicates (clays) for designing flame retardant polymer nanocomposites. Results showed that the effect of clays is beneficial for retarding flame spread in developing fires, but not at the stage of ignition or in the stage of fully developed fires. Liu *et al.* investigated the impact of the modified alpha-zirconium phosphate on the flame retardancy of PLA and found such nanomaterials greatly reduced the flammability of PLA [6]. Hapuarachchi and Peijs [7] utilized the special properties of sepiolite (Sep) and multiwalled nanotubes (MWNTs) to improve the fire performance of PLA, showing obvious reduction of heat release capacity (HRC) for the Sep and MWNTs-based PLA ternary composites, along with significant improvements in residual char. Cheng *et al.* [8] also developed PLA nanocomposites incorporating ATH and modified montmorillonite (MMT) where intercalated and exfoliated structures of clay in the matrix were achieved; moreover, V-0 rating (UL 94) and melt dripping reduction during combustion of the PLA nanocomposite were obtained. However, these nanofillers are costly.

Cellulose nanocrystals (CNCs) extracted from cellulose, which is the most abundant polymeric material on earth, have some different interesting properties, including their possible use as reinforcing phase in polymeric matrices. The CNCs have high stiffness, very low thermal expansion coefficient, estimated about 10^{-7} K^{-1} [9], high elastic modulus around 150 GPa [10] and low density (approximately 1.57 g cm^{-3}). All of these interesting characteristics permit the use of CNCs as reinforcement phase in thermoplastic and/or thermosetting matrices in a nanocomposite approach. Moreover, cellulose nanocrystals, as they are biodegradable, biocompatible and nontoxic, can be used in many fields [11]. Costes *et al.* [12] studied the flame retardancy of PLA compositions containing phosphorus modified micro-/nano-crystalline cellulose (MCC/NCC). Phosphorus was used either by chemical grafting onto cellulose or by co-additive melt blending by using a biobased phosphorous agent (aluminium phytate). Results showed that the charring effect of MCC/NCC was improved. The addition of 20 wt% of phosphorylated M-CC in PLA matrix allowed reaching the V0 level of UL-94 test, but did not significantly reduce the peak of heat release rate (PHRR). The high specific surface area of NCC was

evidenced to be very helpful in promoting the formation of an excellent charred insulation layer. Recently, Zhao *et al.* [13] improved the flame retardancy of PLA by incorporating a gas-solid biphase flame-retardant N,N'-diallyl-P-phenylphosphonicdiamide (P-AA). The flame retardancy of PLA/P-AA was investigated by limiting oxygen index (LOI), UL94, and cone calorimeter test. It was noted that only 0.5 wt% of P-AA loading increased the LOI value of PLA from 20.5 to 28.4 and passed the UL 94 V-0 rating at thickness of 3.2 mm. Nevertheless, a degradation behavior of PLA matrix induced by P-AA was noted, with an evident decrease of the mechanical and thermal performance of PLA [14]. The use of CNCs as reinforcement could improve these specific properties and, on the basis of these perspective results, in the present work we investigated the fire, mechanical and thermal behaviors of PLA composites combining CNCs with P-AA via a two-steps masterbatch melt extrusion processing method.

2 EXPERIMENTAL

2.1 Materials

Poly(lactic acid) (PLA 3251D), with a specific gravity of 1.24 g/cm^3, a relative viscosity of ca. 2.5, and a melt flow index (MFI) of 35 g/10 min (190 °C, 2.16 kg) was supplied by NatureWorks LLC, USA. Glycidyl methacrylate (GMA), with a density of 1.042 g/mL at 25 °C, and dicumyl peroxide (DCP), with a density of 1.56 g/mL at 25 °C, were supplied by Sigma-Aldrich. PLA pellets were dried in an oven at 40 °C overnight. Microcrystalline cellulose (MCC, dimensions of 10–15 µm) was supplied by Sigma-Aldrich. Phenylphosphonic dichloride (PPDCl, 90%), phenyl dichlorophosphate (95%), allylamine (98%), diethyl ether, diethyl ether and triethylamine (TEA) were purchased from Sigma-Aldrich and used without any further purification.

2.2 Methods

2.2.1 Cellulose Nanocrystal (CNC) Synthesis and Characterization

A CNC suspension was prepared from MCC by sulphuric acid hydrolysis following the recipe used by Cranston [15, 16]. Details were also introduced in our previous study [17]. The CNCs were examined by a field emission scanning electron microscope (FESEM, Supra 25-Zeiss) with an operating voltage at 5kV. A few drops of the CNC suspension were cast onto silicon substrate, dried for 24 h and gold sputtered before the analysis.

2.2.2 Synthesis of Flame Retardant N,N′-Diallyl-P-phenylphosphonicdiamide (P-AA)

The synthesis procedures of P-AA were previously described [13], and the route is presented in Scheme 1 below.

2.2.3 Preparation of Masterbatches (MBs)

In order to determine the effects of processing procedures, CNC and PAA content on the properties of the PLA-based nanocomposites, we considered the possibility of using a masterbatch approach in combination with a reactive compatibilization with glycidyl methacrylate (GMA), that we evaluated as suitable methods for improved dispersion of CNC reinforcement in PLA. According to the results reported in our previous work [17], we decided to fix the content of PLA grafted with GMA (g-PLA), suitable as a compatibilizer in the resultant nanocomposites, at 15 wt% [18] and we identified this system as MB1. Grafting of GMA onto the PLA was performed in a twin-screw microextruder (DSM Explorer 5&15 CC Micro Compounder) in the presence of DCP as initiator. Screw speed of 100 rpm and mixing time of 8 min were used in order to realize the grafting reaction, while a temperature profile of 165–175–180 °C was chosen. In the case of CNC-containing materials, the masterbatch, that we have identified as MB2, was obtained by mixing 3.53 wt% CNC (mixing time 2 min) after 6 min of PLA heating, in order to prevent the thermal degradation of CNC.

2.2.4 PLA Nanocomposite Processing and Sample Preparation

Nanocomposites were manufactured using a twin-screw microextruder as well. Conditions of 100 rpm screw speed, 1 min of mixing time and a kneading temperature of 165–175–180 °C were employed to optimize the material's final properties. The barrel temperature of the injection molding machine was set at 200 °C. The injection pressure was kept constant at 4.0 KPa and the mold temperature was set at 55 °C. The dumbbell-shape samples were prepared by mixing the g-PLA, masterbatch and various amounts of P-AA. Injection molded specimens (bulk samples) were used for evaluation of the mechanical and thermal properties. These formulations are reported in Table 1.

2.2.5 Characterizations

2.2.5.1 Fire Behavior Characterizations

The mixture particles (g-PLA, masterbatch and P-AA) were pressed with different sample modulations in a hot presser (LabPro 400, Fontijne Presses) at 170 °C for 3 min under 30 kN loading pressure, with a preheat for 3 min under 4 kN pre-loading pressure. The specimens of PLA control were prepared by the same procedure. The oxygen index meter (FTT, UK) was used to measure the limited oxygen index (LOI) of the nanocomposites with sheet dimension of $130 \times 6.5 \times 3$ mm^3 according to ASTM D2863-97. Vertical burning test was carried out on a UL 94 Vertical Flame Chamber (Fire Testing Technology, UK) with sheet dimension of $130 \times 13 \times 3.2$ mm^3, according to ASTM D3801–10. Five
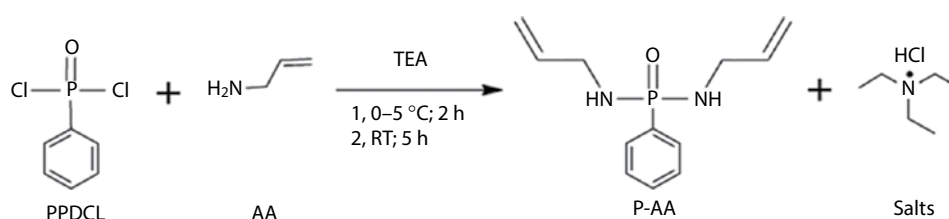
Scheme 1 Synthesis of flame retardant (N,N′-Diallyl-P-phenylphosphonicdiamide [P-AA]).

Table 1 Nanocomposite formulations.

Samples	PLA (%)	MB1 (%)	MB2 (%)	P-AA (%)
Neat PLA	100	0	0	0
PLA/3CNC	0	15	85	0
PLA/3CNC/0.5P-AA	0	15	84.5	0.5
PLA/3CNC/1P-AA	0	15	84	1
PLA/3CNC/2P-AA	0	15	83	2

MB1 = g-PLA
MB2 = PLA+3.53 wt. % CNC

specimens were tested for each composition. Prior to all flammability tests, all the specimens were conditioned at 23 ± 1 °C, for 48 h at 50% RH in a climatic chamber. Micro combustion calorimeter (MCC, Fire Testing Technology, UK) was used to investigate the combustion behavior of P-AA, PLA and intercalated P-AA nanocomposites, according to standard ASTM D7309–13. In this system, 5 mg samples were heated up to 700 °C at a heating rate of 1 °C s^{-1} in a stream of nitrogen flowing at 80 cm^3 min^{-1}. The volatile, anaerobic thermal degradation products in the gas stream were mixed with a 20 cm^3 min^{-1} stream of 20% oxygen and 80% nitrogen prior to entering a 900 °C combustion furnace. The parameters measured from this test are the heat release rate (HRR) in W g^{-1} (calculated from the oxygen depletion measurements) and the total heat release (THR) in kJ g^{-1}.

2.2.5.2 Thermal Properties

Thermal properties of PLA and PLA nanocomposite samples were measured by using a differential scanning calorimeter (DSC, TA Instruments, Q200). Measurements were performed in the temperature range from –25 to 210 °C at 10 °C/min under nitrogen flow, and held at 210 °C for 2 min to erase the thermal history (first scan). After the first heating step, cooling and second heating steps were considered. Thermal parameters obtained from cooling and second heating steps were calculated. Glass transition, cold crystallization and melting temperatures (T_g, T_{cc} and T_m) were determined from the 1st and 2nd heating scans. The crystallinity degree (c) was calculated from the 2nd scan as:

$$\chi = \frac{\Delta H_m}{\Delta H_{m0}\left(1 - m_f\right)} \times 100 \tag{1}$$

where ΔH_m is the melting enthalpy, ΔH_{m0} is the melting enthalpy for a 100% crystalline PLA, taken as 93 J/g [19], and $(1 - m_f)$ is the weight fraction of PLA in the sample.

Thermogravimetric analysis (TGA) was performed using a thermogravimetric analyzer (TGA, Seiko Exstar 6300). Approximately, 8 mg of samples were heated from 30 to 700 °C under air atmosphere at a heating rate of 10 °C/min. The weight-loss rate and maximum thermal degradation temperature (T_{max}) was collected from derivative thermogravimetric (DTG) data. The onset degradation temperature (T_{onset}) was defined as the 5% weight loss drawn from the TG curves after the initial testing temperature, at which the samples begin to degrade. The evolved gaseous products from PLA, PLA/3CNC and PLA/3CNC/1P-AA samples were characterized by coupling thermogravimetry (TA, Q50)

with Fourier transform infrared spectroscopy (Nicolet iS50) (TGA–FTIR). The test procedure for TGA was 10 °C/min from room temperature to 600 °C under nitrogen atmosphere. The evolved gaseous products went through a stainless steel line into the gas cell under nitrogen carrier gas for FTIR detection. The FTIR spectra were recorded in a range of 4000–500 cm^{-1} with a 4 cm^{-1} resolution and averaging 8 scans.

2.2.5.3 Mechanical Behavior

The mechanical performance of neat PLA and PLA nanocomposite systems was evaluated by means of tensile tests (75.0 × 5.0 × 2.0 mm^3, length × width × thickness) on the basis of the ASTM D638 type 5 standard with a crosshead speed of 5 mm/min, a load cell of 10 kN and an initial gauge length of 55 mm. Average tensile strength (σ) and elongation at break (ε_b) were calculated from the resulting stress-strain curves. The elastic modulus (E) was calculated from the initial part of the slope from stress-strain curves. The measurements were done at room temperature and at least five samples were tested for each material.

Dynamic mechanical thermal analysis (DMTA) was carried out using a Rheometric Scientific ARES N$_2$ rheometer in torsion mode. The measurements were performed at a constant frequency of 0.5 Hz with a temperature range from 25 °C to 110 °C at a heating rate of 3 °C/min. Gauge length of 20 mm and strain amplitude of 0.02% were selected. The test specimen dimensions were approx. 30.0 × 5.0 × 2.0 mm^3 (length × width × thickness). The presented data are based on two measurements.

2.2.5.4 Morphological Behavior

Morphological and elemental analysis of the cross sections of the PLA and PLA nanocomposites was performed via field emission scanning electron microscopy (FESEM)/energy-dispersive X-ray spectroscopy (EDS) using a Supra 25-Zeiss instrument with an energy-dispersive X-ray probe attachment (INCA Energy, Oxford, UK). Specimens were cryofractured in liquid nitrogen and the surface was then gold coated. Observation was performed by using an accelerating voltage of 5 kV before the FESEM/EDS observations.

3 RESULTS

3.1 Fire Behaviors

The flammability of PLA and PLA/CNC/P-AA samples was studied by using two small-scale fire tests: limiting oxygen index (LOI) and UL 94 rating tests. The LOI and UL 94 results for PLA and PLA/CNC/ P-AA systems are listed in Table 2.

The PLA control showed a LOI value of 24.0% and achieved a V-2 rating in UL 94 test. The flammability of PLA was slightly enhanced after the addition of 3 wt% CNC. The LOI value of PLA/3CNC was 1 unit lower than that of PLA control and no rating was achieved in a UL 94 test. As reported in our previous study [13], phosphorous containing flame retardant P-AA improved the flame retardancy of PLA with high LOI values and strong self-extinguishing ability in UL 94 test.

In the presence of CNC, the flammability of PLA/CNC/P-AA decreased; compared with PLA/CNC, the LOI value of PLA/CNC/P-AA was increased as the loading of P-AA increased. For instance, the LOI value of PLA/3CNC/1P-AA was 28.8%, which was 5.8 units higher than that of PLA/3CNC. When the loading of P-AA was 2 wt%, the LOI value was increased to 32.3%. In the UL 94 test, with 0.5 wt% loading of

P-AA, PLA/CNC/P-AA passed a V-2 rating. V-0 rating was achieved in both PLA/3CNC/1P-AA and PLA/3CNC/2P-AA. During the test, the dripping of PLA/3CNC/1P-AA or PLA/3CNC/2P-AA was without flame (videos of the UL 94 test were recorded and uploaded as Supplemental Information (SI). The results showed that P-AA endowed PLA with high extinguishing ability.

Cone calorimetry is usually applied to investigate flame retardancy and quantitatively measure heat release in combustion, but it needs high quantities (25–100 g) of materials for accurate and reproducible determinations. MCC is a new, rapid laboratory-scale test, which only requires milligram quantities of materials to measure thermal and chemical properties related to fire. The HRR curves of P-AA, neat PLA and different PLA nanocomposites containing CNC and P-AA, obtained by using the MCC, are given in Figure 1a,b, while PHRR values, collected from the peak of the HRR curves, along with THR and T_{max} values, are summarized in Table 3.

Table 2 LOI and UL94 test results for PLA, PLA/3CNC and PLA/CNC/P-AA nanocomposites.

Samples	LOI (%)	UL94	Phenomena
Neat PLA	24.0	V-2	Dripping with flame, cotton burnt
PLA/3CNC	23.0	NR	Dripping with flame, cotton burnt
PLA/3CNC/ 0.5P-AA	24.5	V-2	Dripping with flame, cotton burnt
PLA/3CNC/ 1P-AA	28.8	V-0	Dripping without flame, cotton not burnt
PLA/3CNC/ 2P-AA	32.3	V-0	Dripping without flame, cotton not burnt

NR: no rating

Table 3 Data recorded during the MCC measurements for of PLA/CNC/P-AA nanocomposites.

Samples	PHRR (W/g)	THR (kJ/g)	T_{max}(°C)
P-AA	166 ± 1	24.9 ± 0.1	288.0 ± 0.5
Neat PLA	448 ± 2	18.5 ± 0.4	392.2 ± 1.1
PLA/3CNC	419 ± 1	17.7 ± 0.2	387.1 ± 1.0
PLA/3CNC/ 0.5P-AA	431 ± 2	18.0 ± 0.2	388.0 ± 0.5
PLA/3CNC/1P-AA	435 ± 1	18.1 ± 0.2	387.4 ± 0.1
PLA/3CNC/2P-AA	447 ± 3	18.3 ± 0.2	388.3 ± 0.8
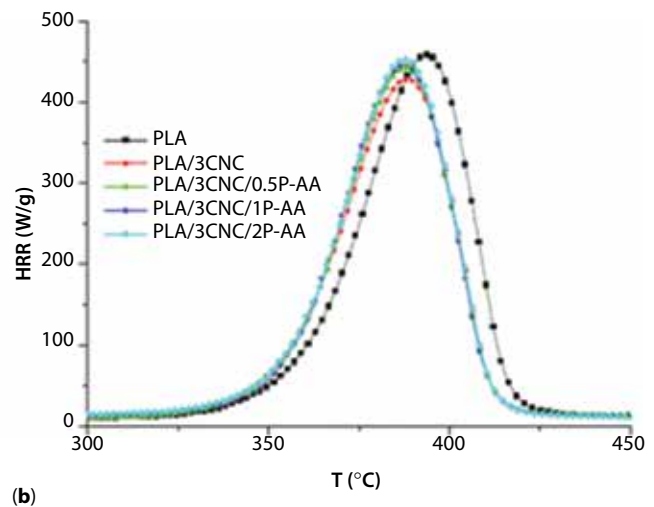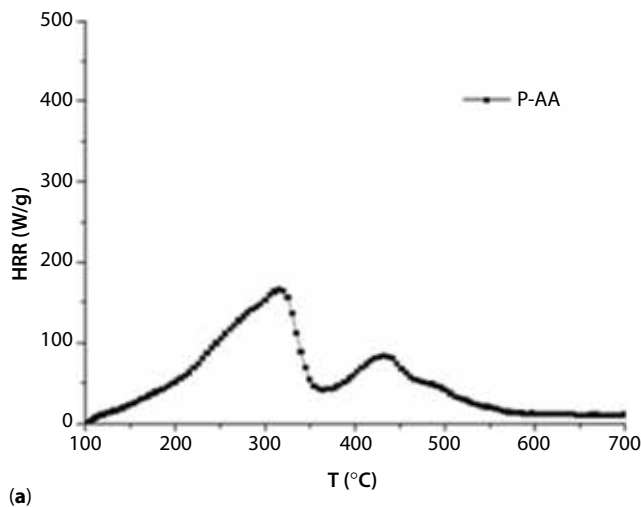
Figure 1 HRR curves of (**a**) P-AA and (**b**) PLA and different PLA nanocomposite systems containing both CNC and P-AA, obtained by microcalorimeter tests.

Compared with PLA control, the PHRR value of PLA/3CNC slightly decreased from 448 ± 2 W/g to 419 ± 1 W/g. The THR value of PLA/3CNC is lower by 4.3% as well. In the presence of P-AA, PLA/CNC/P-AA systems showed PHRR and THR values close to the value of PLA control; for instance, PHRR and THR of PLA/3CNC/1P-AA were 435 ± 1 W/g and 18.1 ± 0.2 KJ/g, respectively, and these decreased values can be considered negligible when compared to PLA control so, in the case of MCC tests, we concluded that the addition of P-AA does not have a significant effect on the fire behaviors of PLA and PLA/CNC systems. However, these results were consistent with our previous findings for cone calorimeter characterization [13]. The different performances of PLA/CNC/P-AA in LOI, UL 94 and MCC tests may be related to the flame-retardant mechanism; it has been observed that P-AA showed a flame inhibition effect in the gas phase [12, 19], while melting and dripping behaviors of PLA/CNC/P-AA in LOI and UL 94 tests are responsible for heat removal from the sample. With these two effects, the LOI value of PLA/CNC/P-AA increased and a V-0 rating was obtained. Nevertheless, in the case of the MCC test, PLA/CNC/P-AA is firstly totally thermally decomposed in N_2, after which all the volatiles will be burnt in the condition of 20% O_2. It means that, under these conditions, the heat decrease caused by melting and dripping behavior in LOI and UL 94 could not be observed, leading to a reduction of the flame inhibition effect of P-AA in PLA/CNC/P-AA and also justifying the behavioral differences in UL 94 and MCC results.

The evolved gaseous products were collected and identified using the TGA-FTIR technique for the purpose of understanding the thermal decomposition behavior of PLA, PLA/3CNC and PLA/3CNC/1P-AA. The products of PLA thermal decomposition mainly consist of CO_2 (2360 cm^{-1}), CO (2184 cm^{-1}), -OH (such as H_2O, 3400-3600 cm^{-1}), hydrocarbons (C-H stretching at 1373 cm^{-1}), aliphatic ethers (1120 cm^{-1}), and compounds bearing a carbonyl group (1760 cm^{-1}) [3, 21]. The major decomposition compounds, obtained during the depolymerization process, are CO_2, H_2O, hydrocarbons, etc. The 3D images of evolved gaseous products of PLA, PLA/3CNC and PLA/3CNC/1P-AA are shown in Figure 2a–c, Panel A, while results of involved gas analysis for PLA/3CNC and PLA/3CNC/1P-AA at maximum decomposition rates are reported in Figure 2a–d, Panel B. Characteristic bands of CO_2 (2360 cm^{-1}), hydrocarbons (-CH_3 and -CH_2- groups, 2980-2850 and 1200–1300 cm^{-1}), and compounds containing carbonyl groups (1760 cm^{-1}) are detected. Meanwhile, it can be observed that the pyrolysis products for PLA/3CNC started to release earlier than neat PLA, and these results are very consistent with results from MCC tests. The absorbance intensity (Total, CO [2184 cm^{-1}] and carbonyl compounds [1760 cm^{-1}]) of pyrolysis products for PLA/3CNC is lower than that for pure PLA. Consequently, the addition of 3 wt% of CNC can decrease the release of combustible gas. This result could be ascribed to the high crystallinity and good dispersion of CNC in PLA matrix, which delayed the production of these products. Surprisingly, the addition of 1 wt% P-AA (PLA/3CNC/1P-AA) did not further reduce the intensity of the pyrolysis products. It is well known that the thermal degradation of polymers is mainly associated with the depolymerization process.

As already reported [14], the thermal decomposition of PLA involved the cis-elimination and random (inter- and intramolecular) transesterification process, which were supposed to be the main reactions under nitrogen condition at high temperature. Moreover, the formed phosphorus-containing acids during the thermal decomposition of P-AA significantly catalyzed the random transesterification in PLA matrix, resulting in the production of more oligomers. Hence, no decrease of the pyrolysis products could be observed when compared with PLA/3CNC.

3.2 Thermal Properties

Figure 3a–c shows DSC thermograms of neat PLA and its nanocomposites during two heating cycles and one cooling scan. The glass transition (T_g), cold crystallization (T_{cc}), melting (T_m) detected from the 1st and 2nd heat scan and crystallinity (χ) calculated from the 2nd scan of PLA and PLA nanocomposites were investigated and summarized in Table 4.

In the 1st heating scan (Figure 3a), the mean value of T_g for neat PLA was 61.3 ± 0.1 °C, while a value of 59.7 ± 0.8 °C was measured for PLA/3CNC: the lower T_g for PLA/3CNC may due to the presence of the g-PLA and some unreacted GMA residual, which served as plasticizer, in accordance with [16]. Moreover, the introduction of flame retardant P-AA resulted in a decrease of T_g, as a T_g value of 56.9 ± 0.1 °C was detected in PLA/3CNC/2P-AA. Meanwhile, the addition of P-AA organic phosphorus structure increased PLA chain mobility, which was also confirmed in [14]. CNC was shown to have a nucleation effect in PLA matrix, as reported in [15, 17, 22, 23], with a reduction in T_{cc} with respect to neat PLA (from 100.7 ± 0.4 to 96.7 ± 0.1 °C after the introduction of 3 wt% of CNC). Interestingly, when the dosage of P-AA increased to 2 wt%, the T_{cc} decreased to 95.7 ± 0.2 °C, and this result could be ascribed to the enhanced PLA chain mobility related to the plasticization effect of P-AA, which further facilitates the formation of crystals [14, 24]. The T_m also decreased with P-AA addition. During the cooling
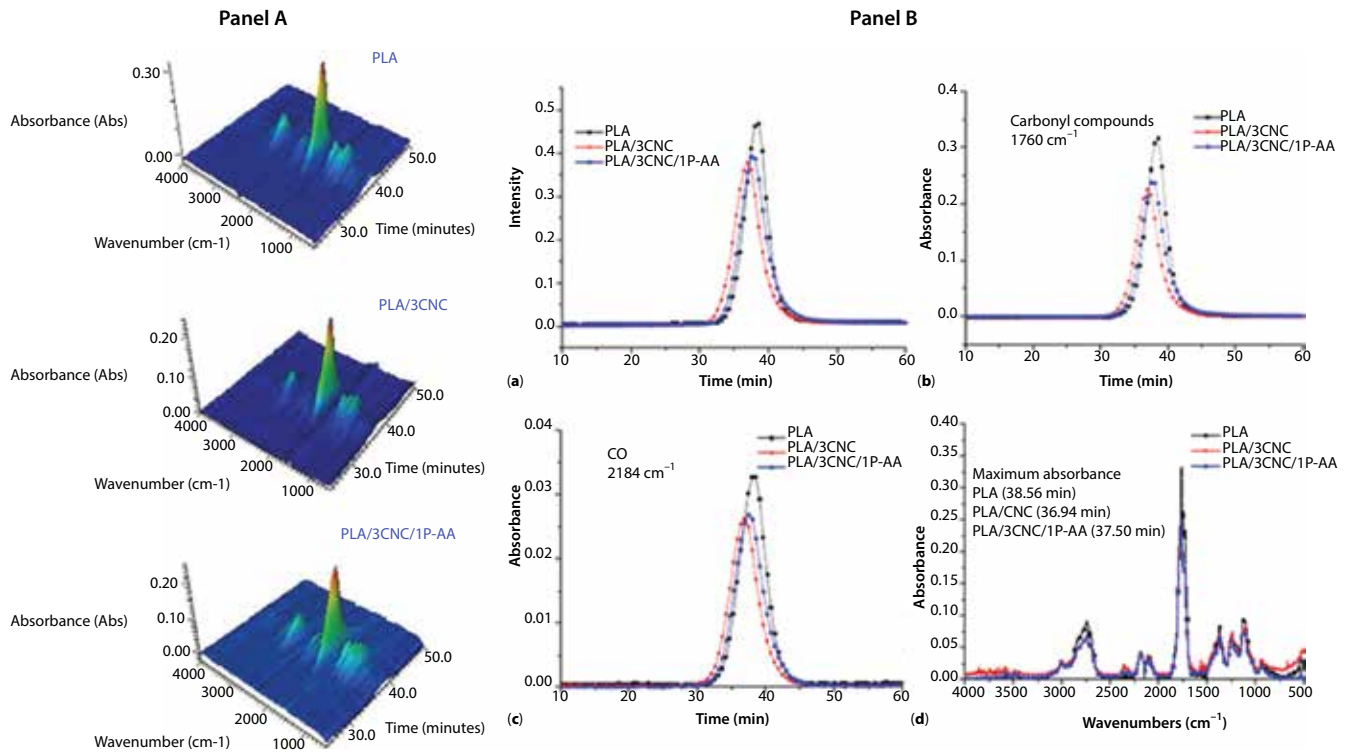
Figure 2 (Panel A) 3D TG-FTIR spectrum of gas phase in the thermal degradation of neat PLA, PLA/3CNC, PLA/3CNC/1P-AA. (Panel B) Absorbance of pyrolysis products for PLA, PLA/3CNC and PLA/3CNC/1P-AA vs time: (**a**) Total, (**b**) Carbonyl compounds, (**c**) CO, and (**d**) Maximum absorbance.

scan shown in Figure 3b, low intensity of exothermic peaks, implying a low crystallization capability, can be observed for the neat PLA. For PLA/3CNC, the exothermic peaks show higher intensity and started from higher temperature with respect to neat PLA, resulting in the enhancement of crystallization capacity. The cellulose nanocrystals were homogeneously dispersed in the PLA matrix and good interaction with the matrix was achieved, which were beneficial for nucleation during the crystallization process of PLA polymer [25]. In the second heating process (Figure 3c), we observed that the T_g, T_{cc} and T_m exhibited a similar tendency, as observed in the 1st heating scan after eliminating the heating history. Due to the combinations of the nucleation effect of CNC and plasticization effect of P-AA, PLA/3CNC/2P-AA showed the highest crystallization capacity, since a value of 16.4 ± 0.1% was detected for crystallinity, almost a two-fold increase in comparison with neat PLA (8.5 ± 1.2%).

The TG and DTG curves of neat PLA and its nanocomposites were recorded in order to evaluate the effect of CNC and P-AA loading on the thermal degradation behavior of resultant composites (Figure 4a,b). The peak values of DTG and the residual weight at 600 °C were also recorded in Table 5. The T_{onset} and T_{max} values of neat PLA were detected at 283 and 328 °C,

respectively. The incorporation of 3 wt% of CNC induced a slight decrease of T_{onset} and T_{max} to 274 and 322 °C, respectively, reducing the thermal stability of the corresponding nanocomposite. This effect seems to be due to the presence of sulphate groups grafted onto CNC surface during sulphuric acid hydrolysis treatment [12]. However, it should be noted that the addition of CNC effectively delayed the thermal degradation progress, since a less sharp DTG curve could be observed in the case of PLA/3CNC when compared with neat PLA. The T_{max} and T_{onset} of the resultant composites increased gradually with the addition of P-AA; 390 and 327 °C were detected, respectively, for PLA/3CNC/2P-AA, indicating that P-AA could be beneficial for the improvement of the system's thermal stability. The use of low content of CNC and P-AA did not significantly increase the residual mass at the end of the test for the corresponding composites.

3.3 Mechanical Behavior

Values for tensile strength (σ) and elastic modulus (E) give an indication of the material's ability to maintain integrity under stress conditions (processing, handling and application). Table 6 shows the results of the tensile test in terms of strength and modulus,
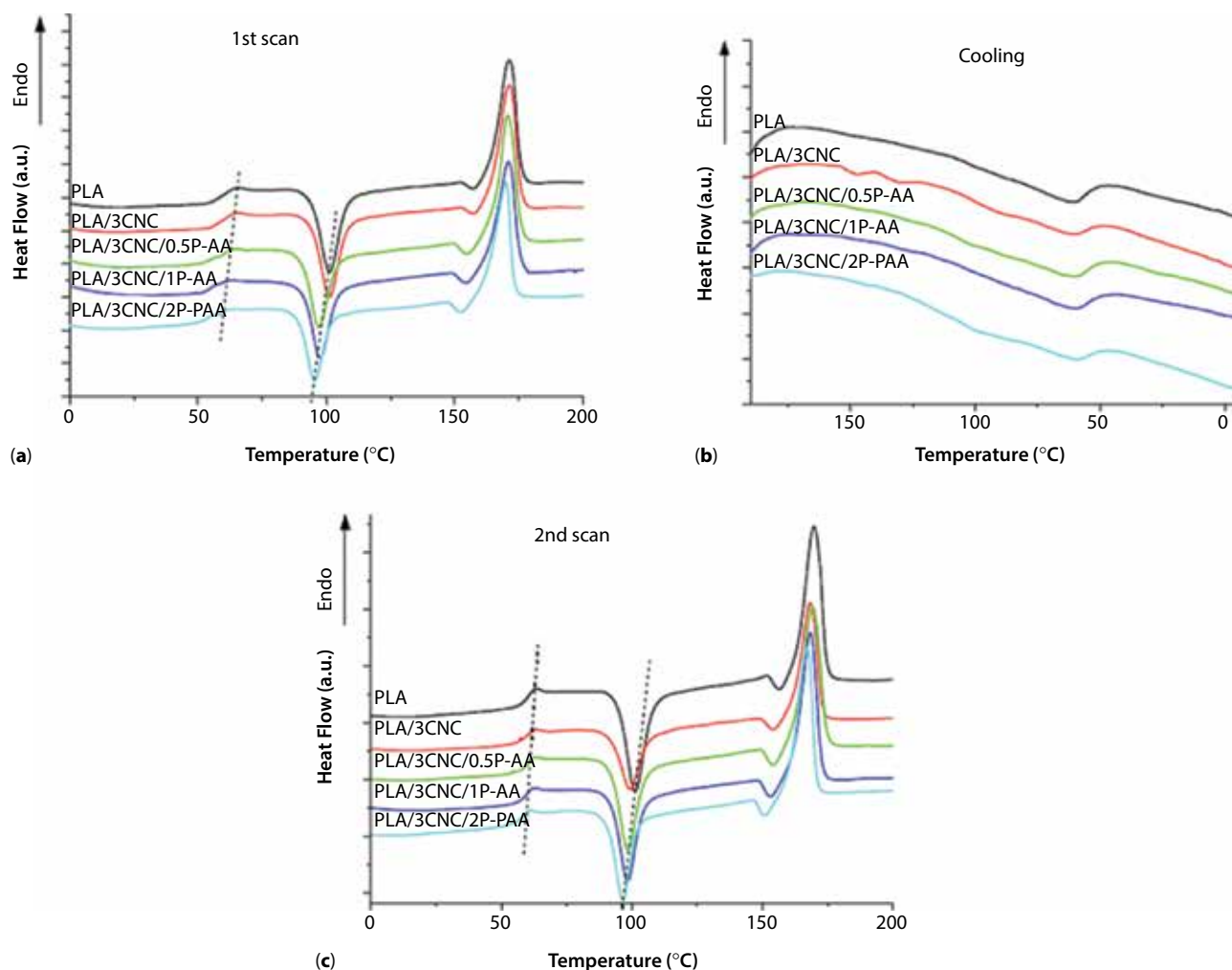
Figure 3 DSC thermograms of PLA and PLA/CNC/P-AA nanocomposites during (**a**) 1st heating scan, (**b**) cooling and (**c**) 2nd heating scan.

Table 4 Thermal parameters (T_g, T_{cc}, T_m) of PLA and PLA/CNC/P-AA nanocomposites (1st and 2nd heating scans).

Samples	1st heating scan			2nd heating scan			
	T_g (°C)	T_{cc} (°C)	T_m (°C)	T_g (°C)	T_{cc} (°C)	T_m (°C)	X_c (%)
neat PLA	61.3 ± 0.1	100.7 ± 0.4	171.4 ± 0.2	60.8 ± 0.1	101.4 ± 0.4	169.2 ± 0.1	8.5 ± 1.2
PLA/3CNC	59.7 ± 0.8	96.7 ± 0.1	170.3 ± 0.2	59.4 ± 1.5	99.2 ± 0.2	168.2 ± 0.1	14.8 ± 1.0
PLA/3CNC/0.5PAA	58.8 ± 0.5	96.5 ± 0.2	170.3 ± 0.5	58.7 ± 0.9	98.3 ± 0.2	168.3 ± 0.4	13.3 ± 0.5
PLA/3CNC/1PAA	57.7 ± 0.2	96.7 ± 0.6	170.4 ± 0.5	58.1 ± 0.2	98.7 ± 0.4	167.5 ± 0.1	13.8 ± 0.2
PLA/3CNC/2PAA	56.9 ± 0.1	95.7 ± 0.2	167.7 ± 0.3	57.3 ± 0.6	96.7 ± 0.1	167.0 ± 0.1	16.4 ± 0.1

while the typical stress-strain curves for all studied materials are reported in Figure 5a, from which it is clear that all the studied samples broke after reaching the yield point. Tensile strength and modulus of neat PLA were 67.2 ± 1.2 and 2792 ± 212 MPa, respectively.

The addition of 3 wt% of CNC (PLA/3CNC) resulted in σ and E reaching 70.3 ± 0.9 and 3599 ± 89 MPa, a 4.6% and 28.9% increase over the neat PLA, which was consistent with our previous studies [17]. The important improvements in elastic modulus could be

Table 5 TGA results for PLA/CNC/P-AA nanocomposites.

Formula	T_{onset} (5%) (°C)	T_{max} (°C)	Residue at 600 °C (%)
Neat PLA	283	328	0.8
PLA/3CNC	274	322	2.4
PLA/3CNC/0.5P-AA	277	324	2.4
PLA/3CNC/1P-AA	282	327	3.1
PLA/3CNC/2P-AA	390	327	3.0

T_{onset}: the temperature at 5% of weight loss.

Table 6 Results of tensile tests for PLA and PLA/CNC/P-AA nanocomposites.

Samples	E (MPa)	σ (MPa)	ε_b (%)
Neat PLA	2798 ± 212	67.2 ± 1.2	3.58 ± 0.17
PLA/3CNC	3599 ± 89	70.3 ± 0.9	2.48 ± 0.07
PLA/3CNC/0.5P-AA	3597 ± 76	68.5 ± 0.7	2.56 ± 0.10
PLA/3CNC/1P-AA	3478 ± 64	66.5 ± 1.1	2.40 ± 0.11
PLA/3CNC/2P-AA	3499 ± 58	64.3 ± 1.8	2.20 ± 0.10
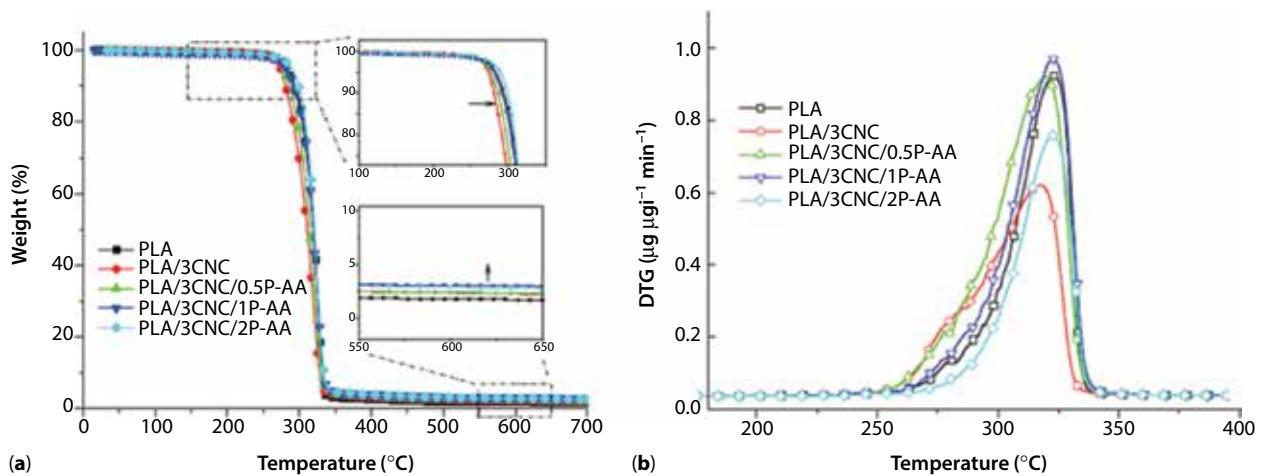
Figure 4 (**a**) TG and (**b**) DTG curves of neat PLA and its nanocomposites containing both CNC and P-AA.
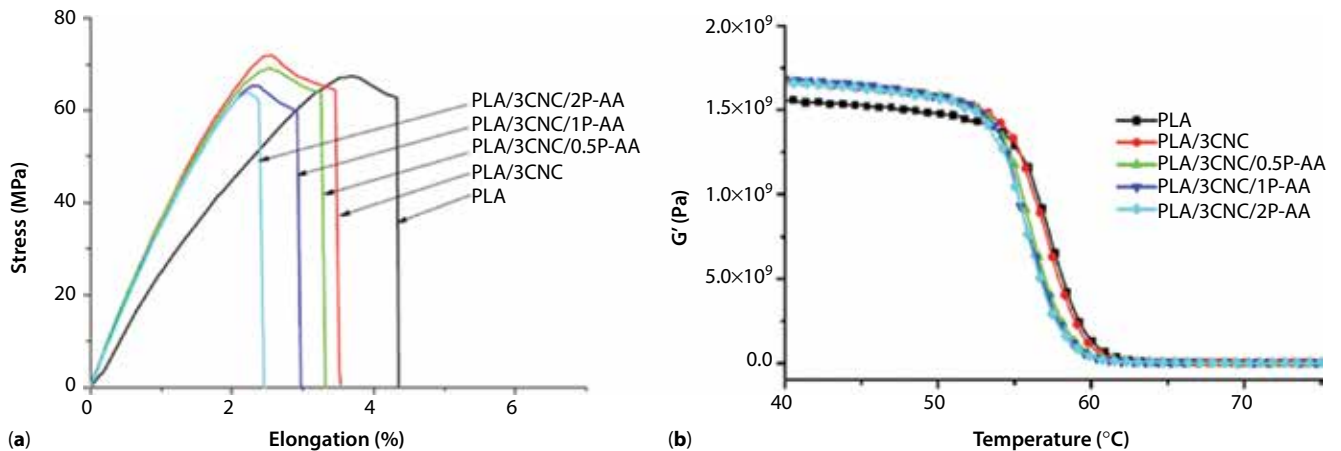
Figure 5 Tensile stress-strain curves of (**a**) PLA and PLA/CNC/P-AA nanocomposites and (**b**) storage modulus as a function of temperature for PLA and PLA/CNC/P-AA nanocomposites.

attributed to the enhanced crystallization behavior confirmed by DSC thermograms discussed above. The addition of P-AA induced a gradual decreasing tendency for σ (from 68.5 ± 0.7 to 64.3 ± 1.8 MPa) and E (from 3599 ± 89 to 3499 ± 58 MPa) of the final nanocomposites, respectively, with increasing P-AA dose

from 0.5 to 2 wt%. These results are consistent with thermal decomposition of the material during the melt-extrusion process, as previous reported [14]. The decrease due to thermal decomposition was negligible, since a remarkable improvement in E (3499 ± 58 MPa in the PLA/3CNC/2P-AA case) was still maintained

due to the presence of the high performing CNC, that was able to recover the deteriorated tensile properties of P-AA containing systems.

3.3.1 DMTA Test

Figure 5b shows the tendency of storage moduli as a function of temperature for the studied materials, while in Table 7 the values of G′ at 30 °C and temperature values for tan d are reported. Generally, it is possible to see that the PLA has a transition around 55 °C. The storage modulus of PLA is increased when 3 wt% of CNC is introduced. The registered values for storage moduli of PLA and the nanocomposites at 30 °C support the data obtained from tensile testing, highlighting the reinforcement effect exerted by CNC. Indeed, as reported in Table 7, measured values for tan delta peak temperature was approximately constant. The peak position for PLA was measured at
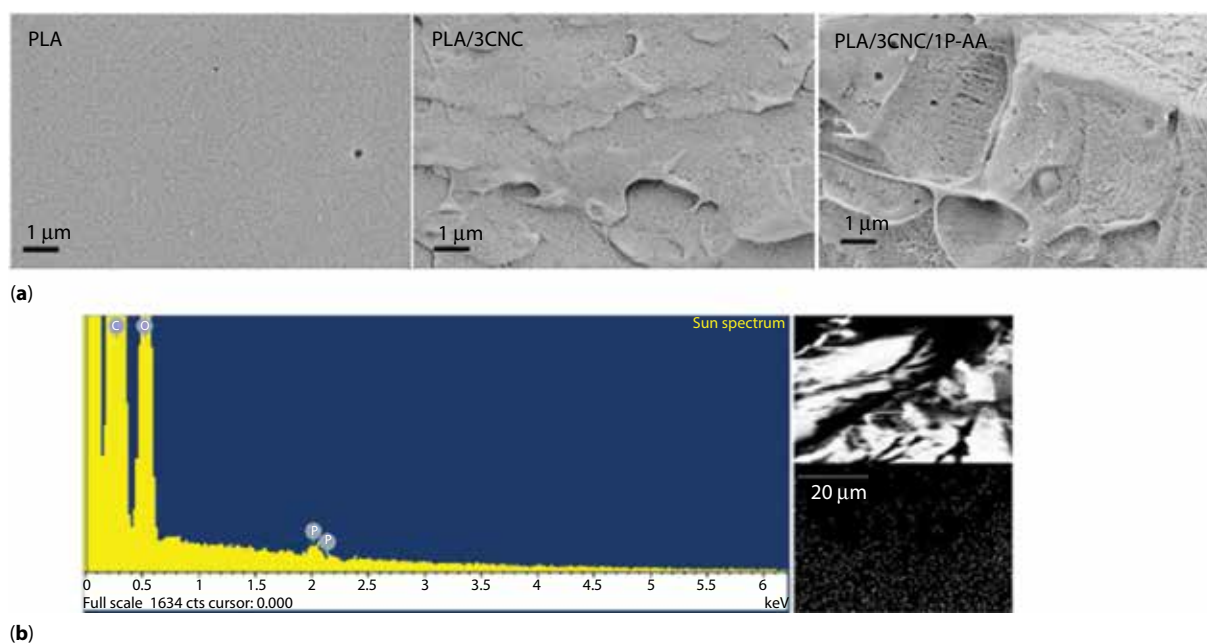
Table 7 Storage modulus and tan delta peak temperatures of PLA and PLA/CNC/P-AA nanocomposites.

Samples	E' at 30 °C (MPa)	$Tan\ \delta$ peak (°C)
Neat PLA	1602 ± 50	63.3 ± 0.2
PLA/3CNC	1711 ± 80	63.0 ± 0.1
PLA/3CNC/ 0.5P-AA	1700 ± 100	63.0 ± 0.3
PLA/3CNC/1P-AA	1728 ± 90	62.0 ± 0.2
PLA/3CNC/2P-AA	1705 ± 100	62.0 ± 0.5

63.3 ± 0.2 °C and was reduced to 62.0 ± 0.5 °C for the PLA/3CNC/2P-AA nanocomposite, which was consistent with the results from DSC tests, although the variation, as expected, is not so significant in DMTA measurements. This indicates that more polymer chains are participating in this transition, enhancing the PLA chain mobility and facilitating the crystallization, in agreement with the DSC test.

3.4 Morphological Behavior

The FESEM micrographs of cross-fractured surfaces for neat PLA and PLA nanocomposites are shown in Figure 6a. A smooth fractured surface could be observed in neat PLA. A rougher surface for the nanocomposite (PLA/3CNC) was measured, when compared with the neat PLA, which evidenced a more brittle property of this material. However, no microdomains can be seen in the studied materials, confirming that optimal CNC distribution at the selected weight amount (3%) in PLA matrix was achieved, due to the optimized processing procedures and the use of GMA. The addition of 2 wt% of P-AA leads to a tougher surface when compared with PLA/3CNC, evidencing the tensile difference among the studied nanocomposites. Figure 6b shows the SEM/EDS mapping results of the PLA/3CNC/2P-AA case. The bright dots reflect the phosphorus atoms and no phosphorus aggregates could be observed, which also confirm the good dispersion of P-AA in PLA.

Figure 6 (a) FESEM images of cryofractured cross sections for neat PLA, PLA/3CNC and PLA/3CNC/1P-AA systems. (b) EDX spectrum and phosphorus elemental distribution from SEM/EDS mapping for PLA/3CNC/2P-AA.

4 CONCLUSIONS

In this study, fire retarding PLA nanocomposites with various contents of N,N′-diallyl-phenylphosphoricdiamide (P-AA) were prepared via a two-steps masterbatch melt extrusion processing method, i.e., glycidyl methacrylate grafting onto PLA matrix and CNC premixing with PLA. The nanocomposites were investigated by fire, mechanical and thermal performances. Results show the value of LOI increased to 28.8% and a V-0 rating in the UL94 test was obtained when adding 1 wt% of P-AA. Meanwhile, the nucleation effect of CNC and plasticization effect of P-AA enhance the crystallization capacity of PLA, since PLA/3CNC/2P-AA showed the highest crystallization capacity of 16.4 ± 0.1%. Consequently, high crystallinity and good dispersion of CNC in PLA matrix delayed the production of pyrolysis products, such as CO and carbonyl compounds, detected by MCC and TG-FTIR, and reduced the THR. Tensile tests and DMA results showed that CNC notably improved the mechanical performance (tensile strength and elastic modulus) of P-AA containing PLA nanocomposites.

ACKNOWLEDGMENT

REFERENCES

1. J. Zhan, L. Song, S. Nie, and Y. Hu, Combustion properties and thermal degradation behavior of polylactide with an effective intumescent flame retardant. *Polym. Degrad. Stab.* **94**, 291–296 (2009).

2. B. Gupta, N. Revagade, and J. Hilborn, Poly(lactic acid) fiber: An overview. *Prog. Polym. Sci.* **32**, 455–482 (2007).

3. X. Wang, Y. Hu, L. Song, S. Xuan, W. Xing, Z. Bai, and H. Lu, Flame retardancy and thermal degradation of intumescent flame retardant poly(lactic acid)/starch biocomposites. *Ind. Eng. Chem. Res.* **50**, 713–720 (2010).

4. S. Bourbigot and G. Fontaine, Flame retardancy of polylactide: An overview. *Polym. Chem.* **1**, 1413–1422 (2010).

5. P. Kiliaris and C.D. Papaspyrides, Polymer/layered silicate (clay) nanocomposites: An overview of flame retardancy. *Prog. Polym. Sci.* **35**, 902–958 (2010).

6. X.Q. Liu, D.-Y. Wang, X.-L.Wang, L. Chen, and Y.Z. Wang, Synthesis of organo-modified α-zirconium phosphate and its effect on the flame retardancy of IFR poly(lactic acid) systems. *Polym. Degrad. Stab.* **96**, 771–777 (2011).

7. T.D. Hapuarachchi and T. Peijs, Multiwalled carbon nanotubes and sepiolite nanoclays as flame retardants for polylactide and its natural fibre reinforced composites. *Compos. Part A Appl. Sci. Manuf.* **41**, 954–963 (2010).

8. K.-C. Cheng, C.-B. Yu, W. Guo, S.-F. Wang, T.-H. Chuang, and Y.-H. Lin, Thermal properties and flammability of polylactide nanocomposites with aluminum trihydrate and organoclay. *Carbohydr. Polym.* **87**, 1119–1123 (2012).

9. T. Nishino, I. Matsuda, and K. Hirao, All-cellulose composite. *Macromolecules* **37**, 7683–7687 (2004).

10. A. Šturcová, G.R. Davies, and S.J. Eichhorn, Elastic modulus and stress-transfer properties of tunicate cellulose whiskers. *Biomacromolecules* **6**, 1055–1061 (2005).

11. Y. Habibi, L.A. Lucia, and O.J. Rojas, Cellulose nanocrystals: Chemistry, self-assembly, and applications. *Chem. Rev.* **110**, 3479–3500 (2010).

12. L. Costes, F. Laoutid, F. Khelifa, G. Rose, S. Brohez, C. Delvosalle, and P. Dubois, Cellulose/phosphorus combinations for sustainable fire retarded polylactide. *Eur. Polym. J.* **74**, 218–228 (2016).

13. X. Zhao, F.R. Guerrero, J. Llorca, and D.-Y. Wang, New superefficiently flame-retardant bioplastic poly(lactic acid): Flammability, thermal decomposition behavior, and tensile properties. *ACS Sustain. Chem. Eng.* **4**, 202–209 (2015).

14. X. Zhao, S. de Juan, F.R. Guerrero, Z. Li, J. Llorca, and D.-Y. Wang, Effect of N,N′-diallyl-phenylphosphoricdiamide on ease of ignition, thermal decomposition behavior and mechanical properties of poly (lactic acid), *Polym. Degrad. Stab.* **127**, 2–10 (2016).

15. E. Fortunati, I. Armentano, Q. Zhou, A. Iannoni, E. Saino, L. Visai, L.A. Berglund, and J.M. Kenny, Multifunctional bionanocomposite films of poly(lactic acid), cellulose nanocrystals and silver nanoparticles. *Carbohydr. Polym.* **87**, 1596–1605 (2012).

16. E.D. Cranston and D.G. Gray, Morphological and optical characterization of polyelectrolyte multilayers incorporating nanocrystalline cellulose. *Biomacromolecules* **7**, 2522–2530 (2006).

17. W. Yang, F. Dominici, E. Fortunati, J.M. Kenny, and D. Puglia, Melt free radical grafting of glycidyl methacrylate (GMA) onto fully biodegradable poly(lactic) acid films: Effect of cellulose nanocrystals and a masterbatch process. *RSC Adv.* **5**, 32350–32357 (2015).

18. J. Liu, H. Jiang, and L. Chen, Grafting of glycidyl methacrylate onto poly(lactide) and properties of pla/starch blends compatibilized by the grafted copolymer. *J. Polym. Environ.* **20**, 810–816 (2012).

19. O. Martin and L. Avérous, Poly(lactic acid): Plasticization and properties of biodegradable multiphase systems. *Polymer* **42**, 6209–6219 (2001).

20. N. Lesaffre, S. Bellayer, G. Fontaine, M. Jimenez, and S. Bourbigot, Revealing the impact of ageing on a flame retarded PLA. *Polym. Degrad. Stab.* **127**, 88–97 (2016). DOI: 10.1016/j.polymdegradstab.2015.10.019.

21. K. Wu, Y. Hu, L. Song, H. Lu, and Z. Wang, Flame retardancy and thermal degradation of intumescent flame retardant starch-based biodegradable composites. *Ind. Eng. Chem. Res.* **48**, 3150–3157 (2009).

22. E. Fortunati, I. Armentano, Q. Zhou, D. Puglia, A. Terenzi, L.A. Berglund, and J.M. Kenny, Microstructure and non-isothermal cold crystallization of PLA composites based

on silver nanoparticles and nanocrystalline cellulose. *Polym. Degrad. Stab.* **97**, 2027–2036 (2012).

23. E. Lizundia, E. Fortunati, F. Dominici, J.L. Vilas, L.M. León, I. Armentano, L. Torre, and J.M. Kenny, PLLA-grafted cellulose nanocrystals: Role of the CNC content and grafting on the PLA bionanocomposite film properties. *Carbohydr. Polym.* 142, 105–113 (2016).

24. S. Saeidlou, M.A. Huneault, H. Li, and C.B. Park, Poly(lactic acid) crystallization. *Prog. Polym. Sci.* **37**, 1657–1677 (2012).

25. A. Pei, Q. Zhou, and L.A. Berglund, Functionalized cellulose nanocrystals as biobased nucleation agents in poly(l-lactide) (PLLA) – Crystallization and mechanical property effects. *Compos. Sci. Technol.* **70**, 815–821 (2010).

Supplementary Document Available Online

http://www.scrivenerpublishing.com/journalsuppl/jrm/JRM-2017-0006/jrm_JRM-2017-0006_supp1.flv

http://www.scrivenerpublishing.com/journalsuppl/jrm/JRM-2017-0006/jrm_JRM-2017-0006_supp2.flv